Soft robot actuators using energy-efficient valves controlled by electropermanent magnets

Citation: Marchese, Andrew D., Cagdas D. Onal, and Daniela Rus. "Soft Robot Actuators Using Energy-efficient Valves Controlled by Electropermanent Magnets." IEEE/RSJ International Conference on Intelligent Robots and Systems (IROS), 2011. 756–761.

As Published: http://dx.doi.org/ 10.1109/IROS.2011.6095064

Publisher: Institute of Electrical and Electronics Engineers (IEEE)

Persistent URL: http://hdl.handle.net/1721.1/72539

Version: Author's final manuscript: final author's manuscript post peer review, without publisher's formatting or copy editing

Soft Robot Actuators using Energy-Efficient Valves Controlled by Electropermanent Magnets

Andrew D. Marchese, Cagdas D. Onal, and Daniela Rus

***Abstract*— This paper presents the design, fabrication, and evaluation of a novel type of valve that uses an electropermanent magnet [1]. This valve is then used to build actuators for a soft robot. The developed EPM valves require only a brief (5 ms) pulse of current to turn flow on or off for an indefinite period of time. EPM valves are characterized and demonstrated to be well suited for the control of elastomer fluidic actuators. The valves drive the pressurization and depressurization of fluidic channels within soft actuators. Furthermore, the forward locomotion of a soft, multi-actuator rolling robot is driven by EPM valves. The small size and energy-efficiency of EPM valves may make them valuable in soft mobile robot applications.**

I. INTRODUCTION

Soft actuators bring both power and natural fluidity to robots. These actuators offer high power to weight ratio in conjunction with compliance, enabling robots to carefully apply high forces to their environments. Additionally, compliance offers inherent adaptability and forgiveness, desirable characteristics in uncertain and dynamic environments.

Construction and operation of soft pneumatic actuators are relatively simple and robust. The actuators are made of elastomer films with embedded fluidic channels and operate by the expansion of these compliant channels under pressure [2].

There are numerous ways to drive soft actuators in robotic applications. Switching PWM valves have been used in the control of pneumatic rubber actuators [3][4]. Here, PWM input of the valve controls flow to the actuator. Additionally, servo valves have been used in the control of soft fluidic actuators for assistance robots [5] and in locomoting robots [6].

Furthermore, solenoid valves were used to drive the bubbler actuator [7], a soft silicone actuator, and its predecessor the tetra chamber actuator [8]. Pneumatic, flexible microactuators have been developed [9] and used in conjunction with solenoid valves in the locomotion of an earthworm-like robot [10]. Also, a spherical robot with exterior inflatable cells utilized solenoid valves to drive locomotion [11]. In these cases, opening of a solenoid valve enables supply pressure to be realized within the actuator.

Methods for driving soft pneumatic actuators can consume substantial real estate, weight, and energy. These are important considerations especially in mobile, multi-segment robots intended for field tasks. The authors present a technology for use in driving soft actuators that can potentially overcome the limitations of currently used mechanisms. The authors employ novel electropermanent magnet (EPM) valves to drive actuation of a soft, multi-segment rolling robot. The low energy consumption of permanent magnet valves has been noted [12] [13]. When used in driving soft actuators, EPM valves can be compact, light weight, and energy efficient.

This work was supported by Defense Advanced Research Projects Agency (DARPA) Grants W911NF-08-C-0060 (Chemical Robots) and W911NF-08-1-0228 (Programmable Matter) and Boeing Company. We are grateful for this support.

A. Marchese, C. D. Onal, and D. Rus are with the Computer Science and Artificial Intelligence Laboratory, Massachusetts Institute of Technology, Cambridge, MA 02139, USA {andy, cagdas, rus}@csail.mit.edu

II. SOFT ROBOT DRIVEN BY EPM VALVES

We designed and built a soft, multi-actuator rolling robot driven by EPM valves. The robot uses several elastomer fluidic actuators around its perimeter to achieve forward motion. Increasing pressure within the fluidic channels extends the surrounding elastomer, displacing the actuator. EPM valves are utilized to drive pressurization and depressurization of the actuators' channels. The introduced EPM valve has a latched (open) and unlatched (closed) state and provides similar functionality to a solenoid valve.

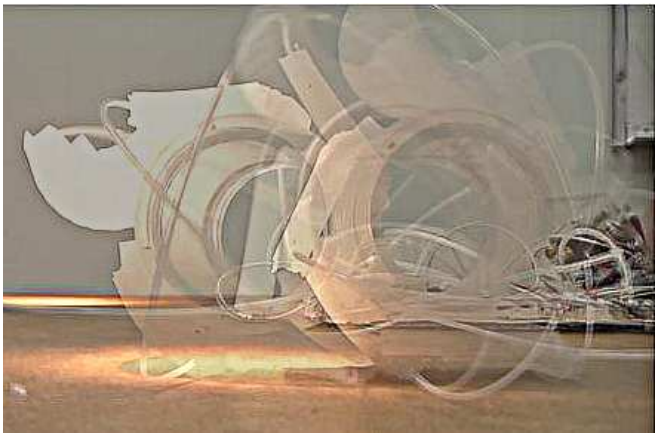

Fig. 1. The soft robot in motion. Fluidic actuators around the robot's perimeter expand under the control of EPM valves, driving the robot forward.

III. EPM VALVE

A. General Principle

Outlet airflow of a check valve is controlled by manipulating the flux output of an electropermanent magnet (EPM). Fig. 2 illustrates the valve's operation. To enable flow in a latched state, a pulse of current, *i*, is applied through a coil (1) around a magnet composed of both AlNiCo (2a) and

NeFeB (2b). The pulse of current orients the two magnets in the same direction, and the total magnetic flux is channeled through the ferrous core material (3). Consequently, a soft ferrous ball (5) placed within a plastic tubing (4) is attracted to the core material and pulled to the side of tubing away from the orifice. In this latched configuration, flow can pass freely through the valve.

To achieve an unlatched state, current is pulsed through the coil in the opposite direction. An impulse of current in this direction orients the magnets in opposite directions in a canceling configuration and flux recirculates among the magnets. Consequently, no flux is channeled through the magnetic core and no magnetic force acts on the soft ferrous ball. The check valve is allowed to follow its original operation, whereby a drag force acting on the ball due to initial airflow in combination with pressure behind the ball pushes the ball against the orifice. The outlet is sealed and little to no flow exits the valve.

Note that, a short (5 ms) pulse of current through the coil permanently switches the EPM and the corresponding flux output. Thus, once latched, no additional input energy is required.

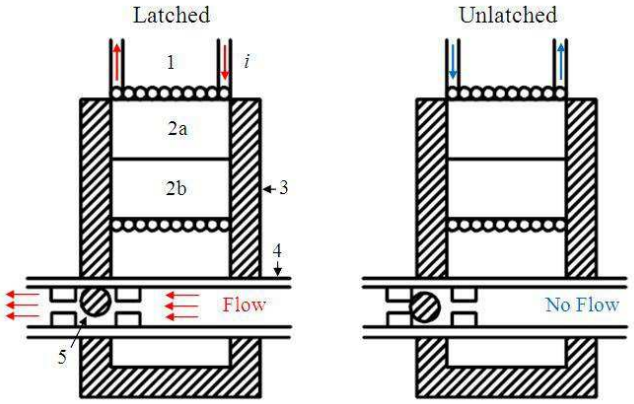

Fig. 2. EPM valve operation. In the latched configuration flow is allowed to pass through the valve. In the unlatched configuration little to no flow exits the valve.

B. Role of EPM

The electropermanent magnet enables flux in an air gap to be toggled on or off. The magnet is composed of cast AlNiCo grade 5 and NeFeB N40 permanent magnet materials arranged in a parallel configuration. AlNiCo and NeFeB materials have a coercivity of approximately 52 and 980 kA/m, respectively.

As a result, AlNiCo's magnetic poles can be reversed with a relatively low external magnetic field compared to the field required to switch the poles of NeFeB. Accordingly, in the latched configuration, the applied magnetic field aligns the two poles, channeling the AlNiCo flux, ϕ_A, and NeFeB flux, ϕ_N, into the ferrous core and through the air gap. In the unlatched configuration, the applied external field orients the AlNiCo poles opposite the NeFeB poles and flux is confined to circulate within a loop, avoiding the air gap [1][14]. the The latched and unlatched flux paths are detailed in Fig. 3.

To switch the poles of AlNiCo, the applied current pulse's peak magnitude must establish an external magnetic field within the coil approximately four times the material's coercivity [15]. Pulse duration is primarily determined by the time constants of the undriven, overdamped LRC circuit used to generate peak current.

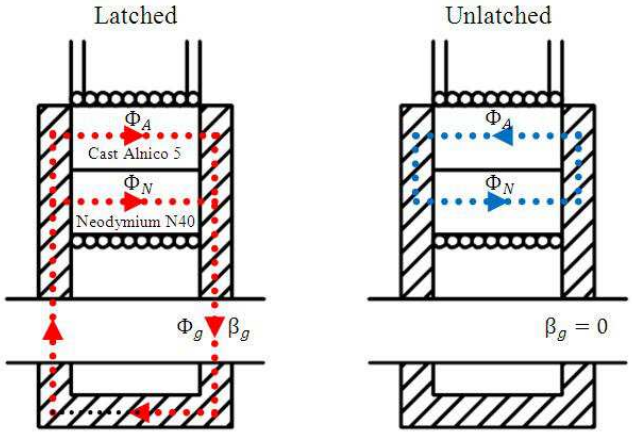

Fig. 3. Flux pathways are depicted. In the latched configuration, flux is routed through the ferrous core material and into an air gap. In the unlatched configuration, flux is confined to circulate between the oppositely oriented poles of AlNiCo and NeFeB.

C. Theoretical Analysis

It is desired to minimize valve dimensions while maintaining the ability to latch and unlatch the valve under operating conditions. Accordingly, a model relating the valve geometry and material properties to the desired outlet flow is developed. Using flux conservation, Strokes' Theorem, and permeability of free space [16][15]:

$$\beta_g ab = \beta_A \frac{\pi d_m^2}{4} + \beta_N \frac{\pi d_m^2}{4}, \quad (1)$$

$$2H_g l_g = H_m l_m, \quad (2)$$

$$\beta_g = \mu_o H_g, \quad (3)$$

can be written, where β_A, β_N, and β_g are the flux densities of AlNiCo, NeFeB, and the air gap, respectively; H_m and H_g are the magnetic field intensities of the magnetic material and air gap, respectively; μ_o is the permeability of free space; and b is the thickness of the ferrous core. Other parameters are detailed in Fig. 4(a).

Combining these equations, the ratio between flux density and magnetic field intensity within the magnetic material can be expressed as:

$$\frac{\beta_A + \beta_N}{H_m} = P_g \frac{4\mu_o l_m}{\pi d_m^2}, \quad (4)$$

where P_g represents the permeance of the air gap. Permeance is the inverse of reluctance. Due to the geometry of the magnetic circuit, flux is not strictly contained within the ferrous core material nor channeled directly through the air gap, but

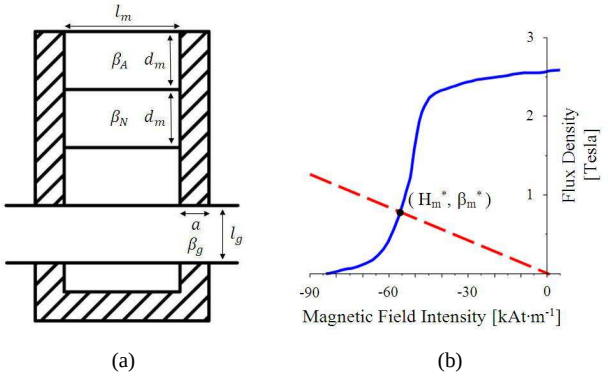

(a) (b)

Fig. 4. Parameters that define the magnetic circuit geometry are shown in (a). Note that, both magnets are assumed cylindrical and equal in size. The combined second-quadrant demagnetization curve of AlNiCo and NeFeB (solid blue) is intersected with a load line (dotted red) to determine the operating point of the magnetic material within the magnetic circuit in (b).

rather leaks through several parallel pathways. According to Herbert Rotor [17], the magnetic circuit's permeance can be calculated by first categorizing each leakage pathway into one of six different geometries, secondly calculating each pathway's permeance in reference to its geometry, and lastly combining permeances for all pathways, including intentional air gaps and fringing pathways, in either series or parallel to resolve an equivalent permeance. The resulting equivalent permeance, P_E in (5), yields the corrected ratio, S, between flux density and magnetic field intensity in the magnetic material.

$$\frac{\beta_A + \beta_N}{H_m} = P_E \frac{4\mu_o l_m}{\pi d_m^2} = S, \tag{5}$$

The intersection of the load line, a line with slope S passing through the origin, and the combined second-quadrant demagnetization B-H curves of AlNiCo 5 and NeFeB N40 yields the operating point, (H^*, β^*), of the magnetic material. Fig. 4(b) displays the intersection of these curves. Using H^* in (2) yields H_g^*. Likewise, β_g^*, the flux density in the air gap can be found using H_g^* in (3). In SI units, the force exerted by the magnet on a ball of diameter d_b within the air gap is:

$$F_m = \frac{\beta_g^{*2} \pi d_b^2}{8\mu_o}. \tag{6}$$

The force on the ball due to drag can be expressed as:

$$F_A = \frac{2\rho d_b^2 C_d \dot{v}^2}{\pi d_T^4}, \tag{7}$$

where ρ is the density of the fluid (air), C_d the drag coefficient for a rough sphere, d_T is the inner diameter of the tubing and $\dot{v}$ is the air flow. F_A is pushing the ball towards the orifice parallel to the tubing and F_m is pulling the ball towards the side of the tube, perpendicular to the air flow. Assuming a static coefficient of friction μ_s between the ferrous ball and the inside wall of the tubing for the ball to successfully latch against the magnetic core in the presence of flow, the following relation should hold:

$$F_A \leq \mu_s F_m. \tag{8}$$

Combining (6), (7), and (8), the minimal level of flux density in the air gap needed to latch and unlatch the ball is given as:

$$\frac{4\dot{v}}{\pi d_T^2} \sqrt{\frac{\mu_o \rho C_d}{\mu_s}} \leq \beta_g^*. \tag{9}$$

Note that, this equation immediately suggests that the required flux density in the air gap does not depend on the ball diameter and has a strong inverse relation to the tube diameter, which means that the mechanism is suitable for scaling down.

D. Model Validation

Several valves of varying geometry were built to verify the model's ability to determine β_g^*, the flux density established in the air gap. Three core widths (1.6, 3.2, and 4.8 mm) and two gap lengths (1.8 and 2.8 mm) were used to generate six flux density measurements. Flux density was measured using a Gauss/Tesla Meter Motel 4048 (Pacific Scientific-OECO, Milwaukee, OR). The probe was placed at both the upper and lower boundaries of the air gap to acquire two different measurements. Fig. 5 illustrates both the model predictions and the actual measurements for each geometry. Model results were consistent with flux densities measured at the upper boundary of the air gap. At a core thickness of 1.6 mm and a gap length of 2.8 mm, 81–50 mT was established in the air gap.

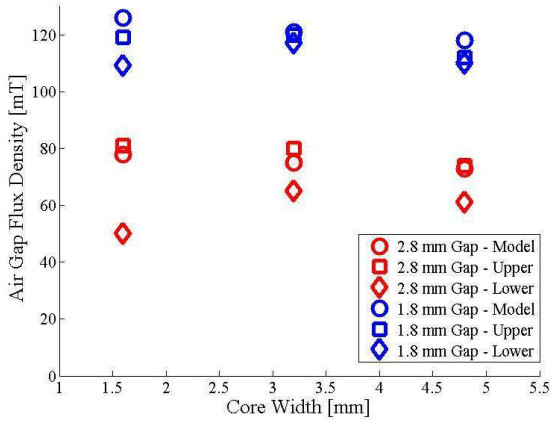

Fig. 5. Three core widths (1.6, 3.2, and 4.8 mm) and two gap lengths (1.8 and 2.8 mm) were used to generate six different valve geometries. Model air gap flux density and measured air gap flux density at upper and lower boundaries of the air gap are reported for each geometry.

E. Valve Characterization

Dynamic characterization of the EPM valve was needed in utilizing such valves to control soft robots. A pressure–flow relationship for the valve in a latched state was experimentally determined. Air flow through the valve was set from 0 to 3.5 lpm in 0.5 lpm increments using a flow meter. A Honeywell pressure transducer (Honeywell Sensing and Control, Golden Valley, MN) was used to measure the resulting pressure difference across the valve. At flows

above 2.0 lpm, valve resistance was observed constant at 0.97 psig/lpm. Fig. 6 displays the EPM valve pressure–flow relationship over a range of operating flows.

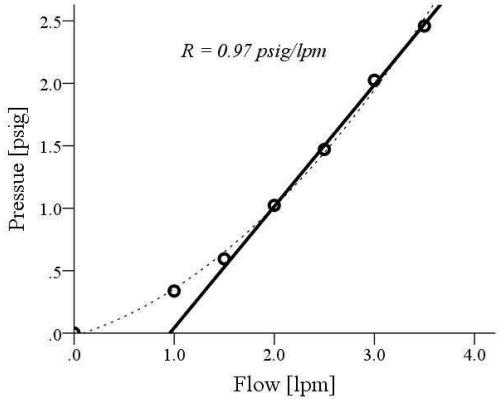

Fig. 6. EPM valve pressure–flow relationship was experimentally determined over a range of operating flows. The dotted line represents measured pressure–flow relationship. Above 2.0 lpm, valve resistance was observed constant at 0.97 psig/lpm, represented by the solid line.

Additionally, the response of flow and pressure to valve latching and unlatching was characterized. Air flow through and pressure across the valve were measured using a Zephyr Analog Airflow Sensor and ASDX Series Pressure Sensor (Honeywell Sensing and Control, Golden Valley, MN). Waveform data was acquired at 5 Hz. An unlatched state is characterized by low flow and high pressure differential, whereas a latched state is characterized by high flow and low pressure differential. Transition from a latched to unlatched state or vice versa occurred within the resolution of our measurement system (0.2 seconds). We observed the state change complete at the measurements directly following the applied current pulse. For our solenoid-like application of EPM valves, this resolution is adequate; however, for a switching application a more precise measurement can be made. Fig. 7 details flow and pressure waveforms during the transition from an unlatched to latched state and from a latched to unlatched state.

IV. EPM VALVE OPERATED SOFT ACTUATORS

A. Design

EPM valves are well suited for driving soft fluidic actuators. Fundamentally, the actuators are made of elastomer films with embedded fluidic channels and operate by the expansion of these channels under pressure. EPM valves can be installed at the inlet and outlet of a channel to control actuator displacement. Fig. 8 illustrates EPM valve placement in the control of a soft actuator.

There are three actuator states, as shown in Fig. 9. When the inlet valve is unlatched and outlet valve latched, little to no flow enters the compliant channel and the internal actuator pressure, P_A, is low relative to the supply pressure, P_S. The mechanism is in its restored state. Initially, when the inlet valve becomes latched and outlet valve unlatched, flow

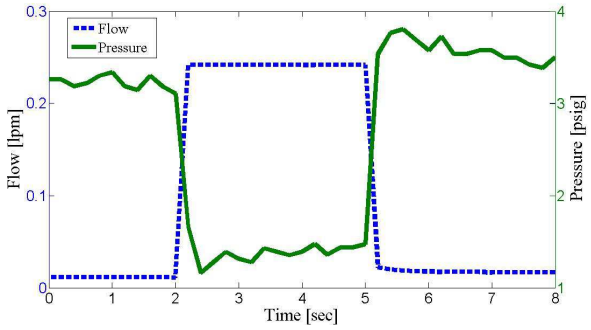

Fig. 7. The response of flow and pressure to EPM valve state transitions. First the valve is transitioned from an unlatched to latched state and secondly from a latched to unlatched state. An unlatched state is characterized by low flow and high pressure differential whereas a latched state is characterized by high flow and low pressure differential.

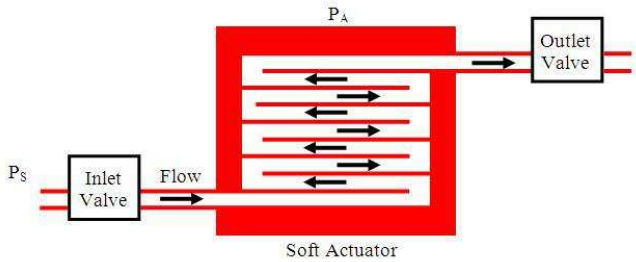

Fig. 8. Inlet and outlet EPM valves arranged to control the displacement of a soft fluidic actuator. P_S is the supply pressure to the actuator and P_A is the internal actuator pressure.

enters the compliant channel and both actuator volume and P_A increase. After sometime P_S and P_A equalize, flow into the channel diminishes, and the actuator reaches steady-state maximum displacement.

B. Experiment

EPM valves were constructed from 3.2 mm dia. by 6.4 mm length AlNiCo (Master Magnetics, Inc., Castle Rock, CO) and NeFeB (K&J Magnetics, Inc., Jamison, PA) magnets. The ferrous core measuring 1.6 mm wide by 3.2 mm thick was constructed from 1018 low carbon steel (McMaster-Carr, Elmhurst, IL). A plastic air tube measuring 3.2 mm O.D. and 2.3 mm I.D. and a soft ferrous ball measuring 1.5 mm O.D. were used. The valve weighed approximately 5 g. The soft actuator measuring 38 mm wide by 38 mm long and 7 mm thick was made from silicone rubber. A supply pressure of 3.5–3.6 psi was used during actuation. Approximately 8–10 mL was delivered to the actuator in 4 seconds. Estimated peak flows of 0.35–0.37 lpm occurred during actuation. Valve dimensions are far from minimally sized considering the operational specifications of the actuator. Under the above dimensions, more than sufficient flux density was generated to latch the ball, 70 mT. Theoretically, the constructed valve can operate in peak flows of 5 lpm. However, at these dimensions valve weight is still reduced, yet the valve is feasible to manufacture with available components.

Actuator	Inlet Valve	Outlet Valve	Inlet Flow	$\Delta P = (P_S - P_A)$
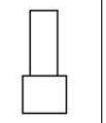	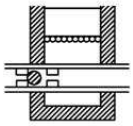	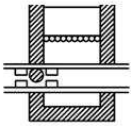	Low	High
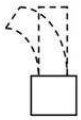	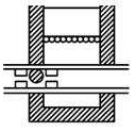	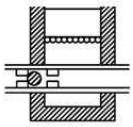	High	Medium
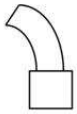	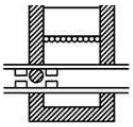	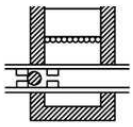	Low	Low

Fig. 9. The soft fluidic actuator's operation can be decomposed into three states. Each state is a function of inlet and outlet valve position and time.

C. Data Analysis

EPM valves successfully controlled soft fluidic actuator displacement. Fig. 10(a) and (b) depict the actuator in its restored and fully displaced states respectively. In Fig. 10(a) the inlet valve is unlatched and outlet valve is latched, P_A is low relative to P_S, and little to no flow is entering the actuator. In Fig. 10(b) the inlet valve is latched and outlet valve unlatched, P_A has equalized with P_S, and flow has finished entering the actuator. Over 5 actuation cycles, mean vertical and horizontal displacement were 19 ± 3.5 and 25.0 ± 0.1 mm respectively. Although horizontal displacement was repeatable, vertical displacement increased with actuation cycle number.

V. SOFT ROBOT LOCOMOTION USING EPM VALVES

A. Mechanism

The forward locomotion of a soft robot consisting of six compliant fluidic actuators was controlled by EPM valves. Fig. 11(a) details the soft robot. The robot was cylindrical in shape and designed to roll forward. Three inlet valves and three outlet valves controlled airflow to three pairs of actuators arranged around the perimeter of the cylindrical chassis. Pairs were placed in opposing locations (1–4, 2–5, and 3–6) and actuated in parallel. Each actuator measured 38 mm wide by 38 mm long and 7 mm thick. By fully displacing the actuator pair in contact with the ground (1–4), the robot is rolled forward, advancing a new actuator pair into contact with the ground (3–6). The two actuator pairs not in contact with the ground remain in a restored state. Fig. 11(b) shows the robot at the end of a step, before the actuator pair is returned to a restored state. This stepping process is repeated, propelling the 180 g robot forward.

B. Experimental Results

Driven by EPM valves, the robot was moved through two complete revolutions, or six steps, on ten different occasions. On average, each step resulted in 53 ± 13 mm of forward travel. Additionally, each step took an average of 8.5 ± 2.5 seconds to complete. Variability in forward travel per step can be attributed to slipping as well as orthogonal components of motion. Step time was primarily influenced by time taken to charge a capacitor in an LRC undriven, overdamped control circuit.

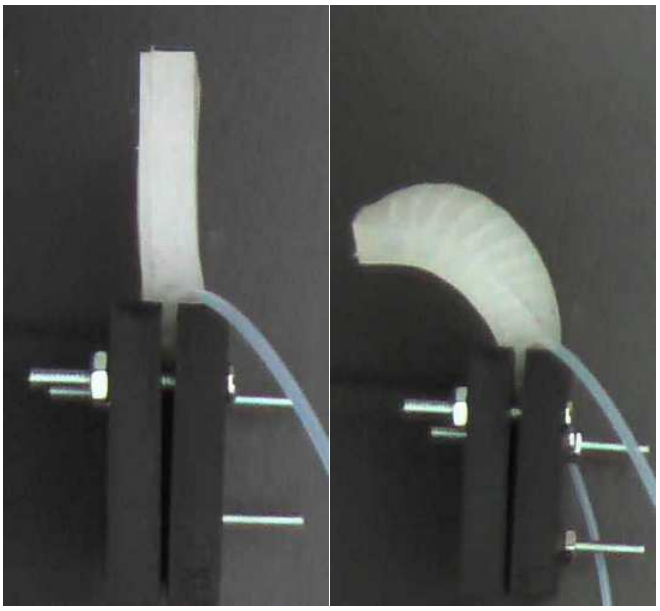

(a) (b)

Fig. 10. Soft fluidic actuator controlled by EPM valves. Depiction of (a) actuator in restored state and (b) actuator in fully displaced state. Vertical and horizontal displacement were 19 ± 3.5 and 25.0 ± 0.1 mm respectively.

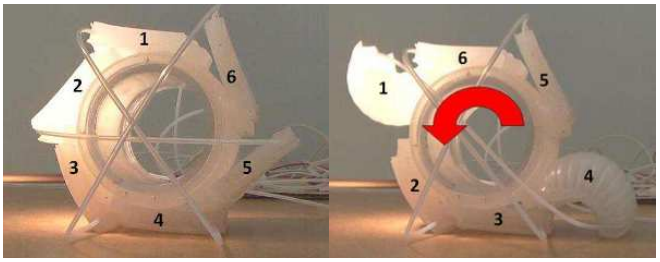

(a) (b)

Fig. 11. EPM valves were used to drive a six segment soft rolling robot. Segments were placed around the perimeter of a cylinder (a). Segments are actuated in pairs, propelling the robot forward and advancing a new pair in contact with the ground (b).

VI. DISCUSSION

EPM valves can effectively drive soft fluidic actuators utilizing only instantaneous pulses of energy to switch actuation states. Although the used valves are relatively small (9.5 mm by 18 mm), they are far from optimally sized considering the operational specifications of the actuators. Further size and power reductions are possible. EPM technology can be used to develop embeddable valves for soft robots. Their

low energy requirements will enhance the longevity and self-sufficiency of mobile robots. Additionally, besides solenoid-like control applications, EPM valves have the potential to be used as switching flow controllers.

REFERENCES

[1] K. Gilpin, A. Knaian, and D. Rus, "Robot pebbles: One centimeter modules for programmable matter through self-disassembly," in *Robotics and Automation (ICRA), 2010 IEEE International Conference on*, May 2010, pp. 2485 –2492.

[2] N. Corell, C. D. Onal, H. Liang, E. Schoenfeld, and D. Rus, "Soft autonomous materials - using programmed elasticity and embedded distributed computation," in *Experimental Robotics (ISER), 2010 International Symposium on*, New Delhi, India, 2010.

[3] Y. Lianzhi, L. Yuesheng, H. Zhongying, and C. Jian, "Electro-pneumatic pressure servo-control for a miniature robot with rubber actuator," in *Digital Manufacturing and Automation (ICDMA), 2010 International Conference on*, vol. 1, 2010, pp. 631 –634.

[4] M. Mihajlov, O. Ivlev, and A. Graeser, "Dynamics and control of a two-link robot arm with soft fluidic actuators for assistance and service applications," in *Robotik, 2008*, Munich, 2008.

[5] M. Jordan, D. Pietrusky, M. Mihajlov, and O. Ivlev, "Precise position and trajectory control of pneumatic soft-actuators for assistance robots and motion therapy devices," in *Rehabilitation Robotics, 2009. ICORR 2009. IEEE International Conference on*, 2009, pp. 663 –668.

[6] K. Suzumori, S. Endo, T. Kanda, N. Kato, and H. Suzuki, "A bending pneumatic rubber actuator realizing soft-bodied manta swimming robot," in *Robotics and Automation, 2007 IEEE International Conference on*, 2007, pp. 4975 –4980.

[7] K. Suzumori and S. Asaad, "A novel pneumatic rubber actuator for mobile robot bases," in *Intelligent Robots and Systems '96, IROS 96, Proceedings of the 1996 IEEE/RSJ International Conference on*, vol. 2, Nov. 1996, pp. 1001 –1006 vol.2.

[8] H. Onoe, K. Suzumori, and T. Kanda, "Development of tetra chamber actuator," in *Intelligent Robots and Systems, 2007. IROS 2007. IEEE/RSJ International Conference on*, Nov. 2007, pp. 777 –782.

[9] K. Suzumori, S. Iikura, and H. Tanaka, "Applying a flexible microactuator to robotic mechanisms," *Control Systems Magazine, IEEE*, vol. 12, no. 1, pp. 21 –27, Feb. 1992.

[10] M. Takahashi, I. Hayashi, N. Iwatsuki, K. Suzumori, and N. Ohki, "The development of an in-pipe microrobot applying the motion of an earthworm," in *Micro Machine and Human Science, 1994. Proceedings., 1994 5th International Symposium on*, Oct. 1994, p. 35.

[11] K. Wait, P. Jackson, and L. Smoot, "Self locomotion of a spherical rolling robot using a novel deformable pneumatic method," in *Robotics and Automation (ICRA), 2010 IEEE International Conference on*, May 2010, pp. 3757 –3762.

[12] I. Yatchev, V. Gueorgiev, K. Hinov, R. Ivanov, and D. Dimitrov, "Dynamic characteristics of a permanent magnet electromagnetic valve actuator," in *Optimization of Electrical and Electronic Equipment (OPTIM), 2010 12th International Conference on*, May 2010, pp. 147 –152.

[13] I. Boldea, S. Agarlita, F. Marignetti, and L. Tutelea, "Electromagnetic, thermal and mechanical design of a linear pm valve actuator laboratory model," in *Optimization of Electrical and Electronic Equipment, 2008. OPTIM 2008. 11th International Conference on*, May 2008, pp. 259 –264.

[14] A. N. Knaian, "Electropermanent magnetic connectors and actuators : devices and their application in programmable matter," Ph.D. dissertation, Massachusetts Institute of Technology, Cambridge, MA, USA, 2010.

[15] A. E. Fitzgerald, C. Kingsley Jr., and S. D. Umans, *Electric machinery (6th ed.)*. New York, NY: McGraw-Hill, 2003.

[16] P. Campbell, *Permanent Magnet Materials and Their Application*. New York, NY: Cambridge University Press, 1994.

[17] L. Moskowitz, *Permanent Magnet Design and Application Handbook. 2nd ed*. Malabar, FL: Krieger Publishing Company, 1995.